Wear 558-559 (2024) 205552

Contents lists available at ScienceDirect

Wear

journal homepage: www.elsevier.com/locate/wear

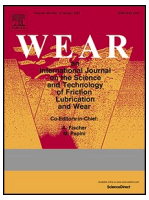

Comparative analysis of pin-on-disc and inertia-dynamometer sliding tests on a friction material

Domenico Antonio Rita [a,*], Stefano Candeo [a], Priyadarshini Jayashree [a], Ana Paula Gomes Nogueira [b], Emiliano Rustighi [a], Giovanni Straffelini [a]

[a] Department of Industrial Engineering, University of Trento, Via Sommarive 9, Trento, Italy
[b] Brembo S.p.A., Stezzano, Italy

ARTICLE INFO

Keywords:
Pin-on-disc testing
Dynamometer testing
Dry sliding
Brake materials
Airborne particulate matter
Vibration phenomena

ABSTRACT

The development of modern brake systems requires the assessment of multiple aspects. Among these, parameters related to the tribological behaviour, vibration, and particulate matter emission are typically evaluated using inertia dynamometers and tribometers. While these two testing systems have been previously compared regarding emissions and tribological behaviours, vibrations were not compared, nor have all these aspects been examined simultaneously. This study investigates the scale effects between a pin-on-disc tribometer and a reduced-scale dynamometer operating under dragging conditions with two levels of pressure and velocity, and a disc temperature not exceeding 260 °C. Regarding the vibration, the pin-on-disc exhibited higher and broader values in the normal direction, 1.3–15.5 m/s^2, than the reduced-scale dynamometer, 0.37–0.42 m/s^2, while the tangential vibrations exceeded those in the normal direction in both systems. The wear rates in the two systems were overall similar, in the range of 1–4 e−14 m^2/N. During the tests the disc temperature in the dynamometer increased at a higher rate compared to the pin-on-disc, affecting the tribological and emission behaviours: steady state values were obtained only in the pin-on-disc tests. The particulate concentration values observed during dynamometer tests better correlated with the peak values from pin-on-disc tests rather than with the steady-state values. This study highlights the importance of including transient values in the evaluation of pin-on-disc testing.

1. Introduction

Performance, particulate emissions, and vibration phenomena are among the many aspects that define the quality and application of modern brake systems. The evaluation of the performances of these systems often involves two different stages: laboratory and field tests, with the latter performed on the actual system in service. Laboratory tests are instead carried out on simpler parameters of the brake system and can be simplified, accelerated, or bench-type [1]. Simplified tests are used as a first screening to rank the performance of different friction materials. The testing rigs used in this stage are reduced-scale systems such as pin-on-disc tribometers, that enable an up-front design for friction materials, usually reproducing only simplified testing conditions, such as dragging conditions. Conversely, full-scale inertia dynamometers belong to the accelerated testing stage, which simulates real operating conditions. Reduced-scale inertia dynamometers, such as those used in Refs. [2–4], provide the advantages of small-scale systems allowing the same operating conditions as full-scale systems. In particular, reduced-scale dynamometers, featuring specimens of standard size and geometry, rule out the influences from other components of the braking system, enabling a prompt examination of frictional contact, irrespective of a specific brake system. In addition, the operating and maintenance of reduced-scale costs are generally lower [2,5,6].

Noise and vibration phenomena generated by braking represent one of the major concerns in brake systems since they can affect safety or drive comfort, leading to a low-quality perception. More than twenty different vibration phenomena are typically found in disc brakes, the most common probably being brake squeal. For example, the work of Balaji et al., among others, summarized in detail the latest NVH-type requirements for brakes [7]. Another side effect of braking is the production of airborne Particulate Matter emissions. It is estimated that brake emissions account for 21 % of all the emissions coming from road traffic [8]. Particles below 2,5 μm in diameter are the most dangerous for human health [9–11]. Nevertheless, relating particulate emissions to

* Corresponding author.
E-mail address: domenicoantonio.rita@unitn.it (D.A. Rita).

https://doi.org/10.1016/j.wear.2024.205552
Received 4 April 2024; Received in revised form 19 July 2024; Accepted 20 August 2024
Available online 22 August 2024

the vibratory phenomena of the braking system is relatively new [12–14].

Several studies compared subscale dynamometers to full-scale dynamometers. They found a good correlation between the reduced-scale and its reference full-scale dynamometer in terms of CoF, even if the hardware effects of the brake corner slightly affect the results [2,5]. However, little research has been done to compare and relate results from a simplified tribometer like the PoD and inertia-dynamometers, whether full-scale or reduced-scale. Veeman et al. [15] stated the importance of conducting tests on both pin-on-disc and brake dynamometer systems, due to their different thermal response. Alemani et al. [16] focused the comparison between a PoD and a full-scale dynamometer on particulate emissions and CoF. Dragging conditions were applied on new and used low-steel samples sliding against a cast iron disc. They confirmed the existence of a transition temperature (TT) that boosts the emissions by one order of magnitude, which is affected by the testing scales and by the frictional pair status. The TT observed in the dynamometer for used samples was nearly twice as high as that observed in the PoD: 380 °C versus 186 °C. In general, the dynamometer showed a higher temperature rise, which was explained by a lower heat dissipation by conduction. Instead, the PoD showed higher values of coefficient of friction (CoF) but similar trends between the two test systems. Federici et al. [17] compared the friction and wear resistance of a PoD and a reduced-scale dynamometer using two friction materials. They found a proportionality in the wear rates of the two testing rigs and a similar CoF.

Nowadays it is fundamental to delimit the application field for the testing equipment used to test friction materials. This permits avoiding the redundancy of the tests, reducing testing times, and concentrating on the development of friction material formulations. This study focuses on two testing rigs that have been scarcely compared in the literature: a pin-on-disc and a reduced-scale inertia dynamometer. It presents an extensive comparison of the tribological, thermal, vibration, and particle emissions of the two systems. Only Federici et al. [17] compared the PoD to a reduced-scale dynamometer, however, without considering the mechanical vibrations.

In this work, each acquired parameter is compared in terms of absolute value, and emphasis is also placed on the sensitivity of the systems to contact pressure and sliding velocity (PV sensitivity). Both systems reproduced dragging conditions with a contact pressure (P) of 1 and 2 MPa, a sliding velocity (V) of 1.5 and 3 m/s, and a maximum disc temperature of approx. 260 °C. The maximum temperature was set to avoid reaching the transition temperature for emissions and maintain the typical surface characteristics of mild sliding conditions. This analysis identified the primary differences between the two systems and their influence on tribological and emission behaviours, with particular attention on the role of disc temperature. Eventually, this work aims to improve general understanding and guide informed decisions regarding tribological testing.

2. Material and methodology

2.1. Materials

In this study, pins and coupons were made of a low-metallic material and were machined directly from commercial brake pads. The elemental composition of the friction material, as obtained from Energy-Dispersive X-ray Spectroscopy (EDXS) analysis, is listed in Table 1. The typical morphology and microstructure of the pad materials with an indication of the main ingredients is shown in the observation by the Scanning Electron Microscopy (SEM), see Fig. 1. The counter face discs were made of pearlitic grey cast iron. The specimens are presented in Fig. 2. Before the tests, the PoD discs were polished thoroughly with a SiC 180 grit abrasive paper. The PoD tribometer mounted a single pin of cylindrical shape together with a disc. The pins had an average height of 9 mm, an average diameter of 10 mm, and an average area of 78.5 mm^2. The dynamometer was equipped with two small pads, referred to as 'coupons', and a disc. The coupons had a combined area of 7.2 cm^2 and were positioned 180° apart. The pad's Shore D hardness was approximately 70. The disc of the PoD had a diameter of 60 mm and a thickness of 6 mm, while the disc of the dynamometer had a diameter of 120 mm and a thickness of 6 mm. The effective radii were 50 mm for the dynamometer and 24 mm for the PoD. The discs had a surface roughness (R_a) of 1.6 ± 0.1 μm, as measured with a stylus profilometer, and an HVC hardness of approximately 210.

2.2. Setup and testing conditions

This study used two testing rigs: a horizontal PoD tribometer (Ducom Instruments, India) and a reduced-scale inertia dynamometer, also called subscale Dyno (LINK model 1200). The systems are depicted in Figs. 3 and 4, along with a description of their main components. The dynamometer can operate brake actions in deceleration or drag mode. Deceleration-mode brake actions reproduce the dynamic events as the applied pressure is controlled to maintain a constant vehicle deceleration while the speed decreases between the initial and final set-point velocities. In drag mode brake actions, on the other hand, the velocity and pressure are controlled to maintain constant values during the set contact time. The PoD tribometers usually operate in drag mode as the velocity is maintained constant during the contact, but they do not have systems to control the load and torque.

Reduced-scale testing has been used to quantify the CoF as a function of several testing parameters in real operating conditions [2]. To ensure that the same braking conditions of a reference vehicle are represented on the subscale dynamometer, a scaling relationship must be set considering the effective radii and the areas of both systems. The parameters held constant between the two systems are the sliding velocity, the contact pressure, and the energy dissipation per unit area, following the energy density approach. To guarantee the equivalence between the specific energies, and thus a comparable disc temperature rise, a scaled inertia has to be mounted on the rotor of the reduced-scale dynamometer [2,4]. Furthermore, the rotor disc in the subscale Dyno is scaled by

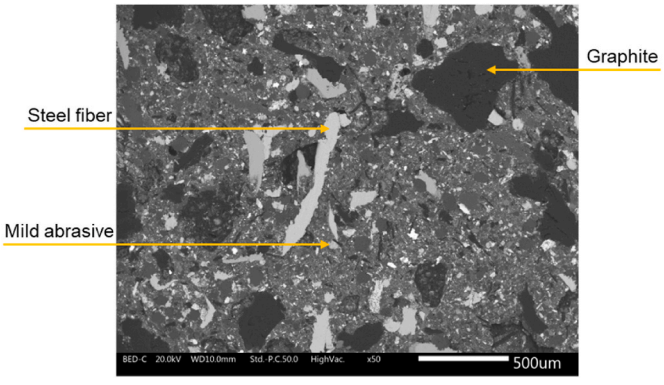

Fig. 1. SEM micrographs of the friction material.

Table 1
Elemental composition of the friction material, as obtained from EDXS (in weight%). The carbon content was not included in the analysis.

Element	O	Fe	Zn	Mg	Al	Sn	Cu	Si	Ca	S	Cr	K
(wt%)	23.8	8.63	13.83	11.92	9.73	8.71	5.33	5.18	4.96	4.9	2.55	0.46

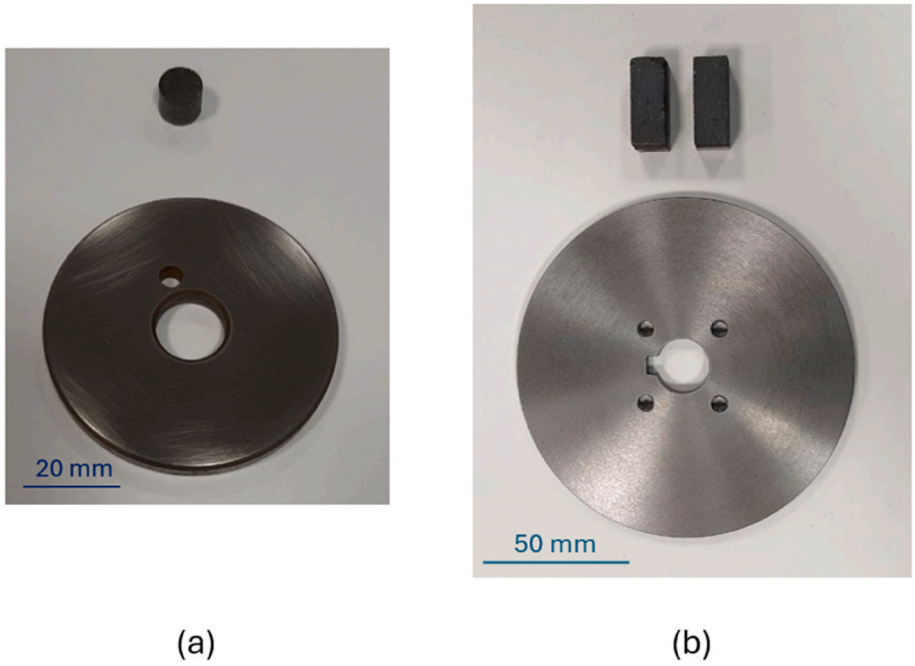

Fig. 2. Specimens: (a) pin and disc for the PoD; (b) coupons and disc for the subscale dynamometer.

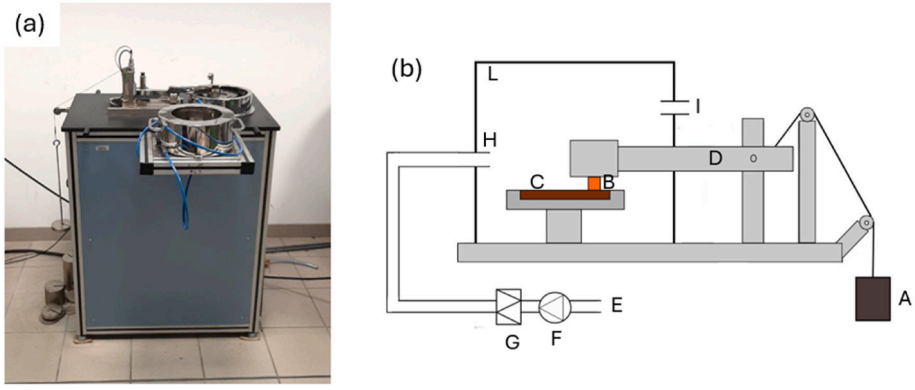

Fig. 3. (a) Pin-on-disc tribometer; (b) Testing apparatus setup: (A) Deadweight, (B) Pin, (C) Disc, (D) Pin holder, (E) ambient air, (F) fan, (G) HEPA filter, (H) air inlet in the chamber, (I) air outlet to the OPS, (L) enclosed chamber for emission measurement.

computing the thermal mass, namely the ratio between the dissipated kinetic energy and the temperature-dependent specific heat of cast iron [2].

The specimens were subjected to dry sliding tests under dragging conditions, i.e. pressures and sliding velocities were kept constant during each application. The tests were conducted with an initial braking temperature between 25 and 50 °C. Two factors, i.e., contact pressure, P, and sliding velocity, V, were varied in the analysis, and two levels were considered for each factor, leading to four different testing parameters, listed in Table 2. The PV factor, reported in the same table, is the product between the nominal contact pressure and the sliding velocity and is generally proportional to the wear and the temperature rise of the contact temperatures. The operating range of the PoD limited the choice for the levels of P and V. The selected testing conditions correspond to a moderate urban braking action, corresponding to approx. a maximum vehicle speed of 30 km/h and the sliding conditions are attained in a mild wear regime [1].

To assess friction, wear, and emission properties, it is essential to ensure a suitable conformity between the surfaces of the samples. This condition was achieved through a bedding stage conducted before the actual testing period. For the PoD, the drag condition at 1.5 m/s and 1 MPa was applied for 30 min. Previous investigations showed that this phase was effective in achieving a conformal contact between the pin and the disc [18,19]. After the bedding stage, the tests were conducted for 90 min, regardless of the applied P and V. This duration assures the establishment of a well compacted and extended secondary contact plateaus, and the achievement of a steady state in emissions and CoF trends [18,19].

The bedding stage of the dynamometer instead consisted of 320 stops at brake pressure of 15–46 bar, vehicle speed of 80-30 km/h, and initial disc temperature of 100 °C [20]. The choice not to surpass a disc temperature of 260 °C, aiming to maintain the typical surface characteristics of mild sliding conditions, limited the testing time of the dynamometer tests to 22 s. Fig. 5 anticipates the thermal evolution over time for the tests at (1 MPa, 1.5 m/s) and at (2 MPa, 3 m/s). It indicates that the temperature rise of the disc during the PoD tests is significantly lower when compared to the dynamometer, an aspect that is further addressed in the 'Discussion' section since it markedly influences the obtained results. Three tests were conducted for each experimental point. In the 'Results' section tables show the average values of the tests for the PoD and the dynamometer, and graphs show the curves that are closer to the average behaviour.

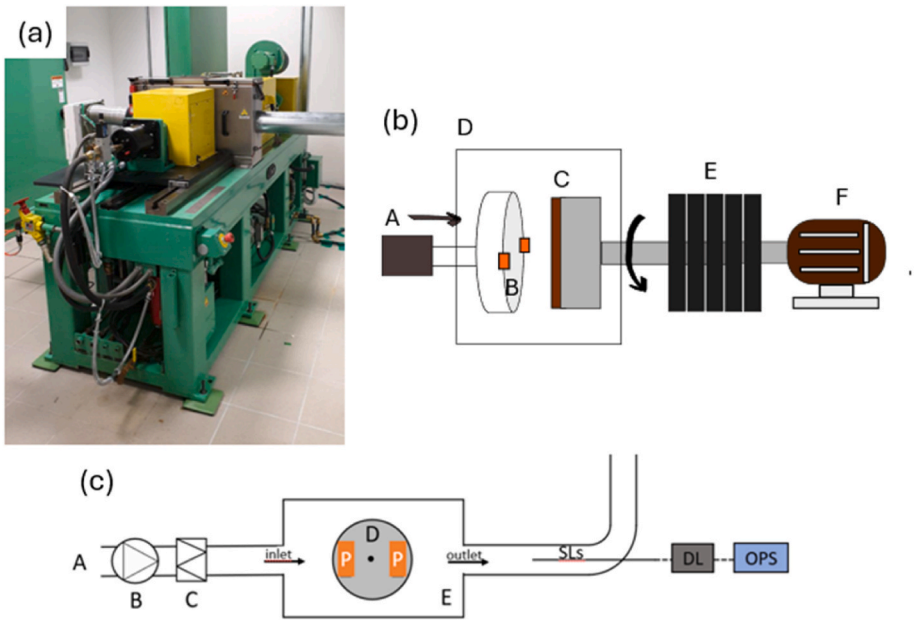

Fig. 4. (a) Subscale dynamometer; (b) Main dyno components: (A) Pneumatic actuator, (B) Coupons, (C) Brake rotor, (D) Enclosed brake chamber, (E) Inertia discs, (F) Electric motor; (c) Testing apparatus for emissions: (A) Ambient air, (B) Fan, (C) HEPA filter, (D) Coupons, (E) Enclosed chamber, (SLs) Sampling line, (DL) Diluter.

Table 2
Testing conditions - parameters.

Testing configuration	Contact Pressure (MPa)	Sliding Velocity (m/s)	PV factor (MPa•m/s)
1	1	1.5	1.5
2	2	1.5	3
3	1	3	3
4	2	3	6

In case of the PoD testing, the CoF was continuously recorded at a sampling rate of 1 Hz, using a load cell that measures the tangential force exerted by the pin holder. In case of the dynamometer tests, the CoF (μ) was calculated by the following relationship:

$$\mu = \frac{F_T}{F_N} = \frac{C_{brake}}{R^S_{eff}} \frac{1}{F_N}$$

where R^S_{eff} is the effective radius of the subscale Dyno, and C_{brake} is the brake torque measured at a sampling rate of 10 sample/s.

The wear resistance of the frictional pair was evaluated in both cases by the specific wear coefficient (K_a), expressed by the Archard relationship [21,22]:

$$K_a = \frac{\Delta V}{F_N\, d}$$

where ΔV is the wear volume loss, F_N is the applied normal load, and d is the sliding distance.

In particular, the wear volume was obtained by dividing the mass loss of the pin, or the coupon, by the material density, 2.2 g/cm^3. The friction materials were weighed before and after the test with an analytical balance with an accuracy of 10^{-4} g.

The temperature of the PoD disc was acquired with a pyrometer, at a sampling rate of 1 Hz. The disc temperature of the subscale dynamometer was acquired at 10 Hz with a k-type thermocouple, which was inserted directly below the disc surface at the effective radius distance. Both temperature sensors were calibrated and had a measurement uncertainty of less than 1 %.

The particle number concentration was measured with an Optical Particle Sizer (OPS), the TSI 3330. The OPS was connected to both testing rigs to measure the concentration of particles in a size between 0.3 and 10 μm. The OPS apparatus had a sampling frequency of 1 Hz and a self-controlled sampling flow rate of 1 l/min. Figs. 3b and 4c depict the schematics for the measurement setup respectively in the PoD and the dynamometer. Both testing rigs featured an air inlet zone and an outlet sampling point, where the OPS collects the sample to be measured. Before entering the enclosed chamber with the samples, the air was filtered through a HEPA filter. However, some parameters were kept different between the two testing rigs. The inlet air velocity of the PoD was set to 11.5 m/s, as determined in Refs. [23,24], leading to an air

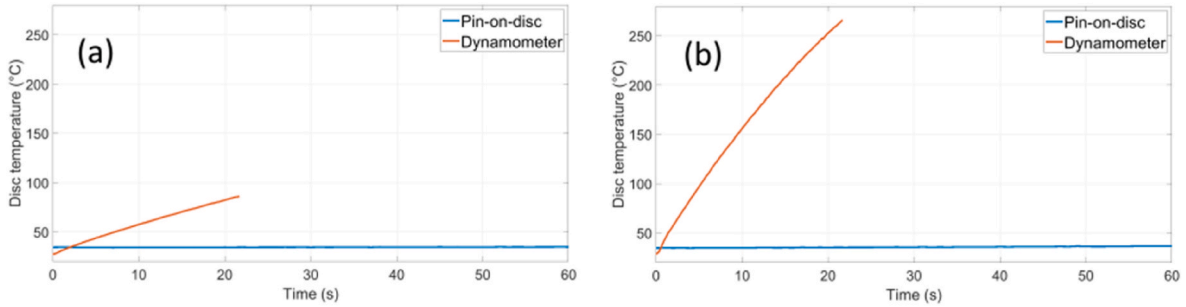

Fig. 5. Comparison of the disc temperature among the different testing rigs: (a) test at (1 MPa, 1.5 m/s); (b) test at (2 MPa, 3 m/s).

flowrate of 14.1 l/min and an air exchange rate inside the chamber of about 1.7 times/min. The apparatus adopted for the PoD is based on the approach developed by Olofsson et al. [25–27]. For the dynamometer the inlet air velocity was set to 1 m/s, leading to an air flowrate of 910 l/min and an air exchange rate of 20 times/min. In addition, the OPS was connected to a diluter, which dilutes the particle concentration by a factor of 10, to guarantee that the measurements fall within the upper limit of 3000 #/ cm^3, as done in Ref. [28]. Moreover, the selection of the nozzle diameter at the sampling point ensured isokinetic conditions for the dynamometer setup. These conditions were not assured on the PoD.

The vibrations of the two systems were acquired using different accelerometers. For the PoD, two single-axis shear accelerometers PCB® Model 352A24, were placed on the pin-holder to measure the normal and tangential accelerations, as shown in Fig. 6a. The nominal sensitivity of the two accelerometers was 100 mV/g. On the other hand, a single triaxial accelerometer PCB® Model HTJ356B01, with a sensitivity of 5 mV/g, was placed at the back plate of one of the two coupons to simultaneously acquire the accelerations in the normal and tangential directions (Fig. 6b). The acquisition of the acceleration data was done through a 'DEWESoft–SIRIUSm' data acquisition system, at a sampling rate of 20 kHz. The root mean square (RMS) value of the acceleration, with a frame size of 1 s, was computed as a representative value for the vibration level of the system. The RMS of the acceleration was computed from the power spectral density of the signal, as follows:

$$a_{RMS} = \sqrt{\sum \mathrm{PSD}(f)\Delta f}$$

where PSD(f) represents the power spectral density of the sampled signal, a function of frequency, while Δf is the frequency resolution, which is determined by the frame size. The RMS describes the energy content of the signal in the time domain.

3. Results

3.1. PoD measurements

Fig. 7 depicts the evolution over time of four parameters for one representative trial of (1 MPa, 3 m/s). Fig. 7a shows that a thermal equilibrium between the disc and the external environment is not reached, since the disc temperature is increasing at the end of the test. A thermal equilibrium was reached only for (1 MPa, 1.5 m/s). Table 3 lists the temperatures reached by the PoD disc at the end of the test. As expected, the tests with the highest PV factor reach the highest temperature. The tests with a 3 MPa m/s PV factor do not exceed 100 °C, while the tests at (1 MPa, 1.5 m/s) reach the lowest temperatures. Table 3 also reports the steady-state values of the PoD testing as an average and standard deviation among the different trials. Five parameters are reported for all the tests: disc temperature, specific wear coefficient of the pin, CoF, total particle concentration, and normal and tangential vibrations.

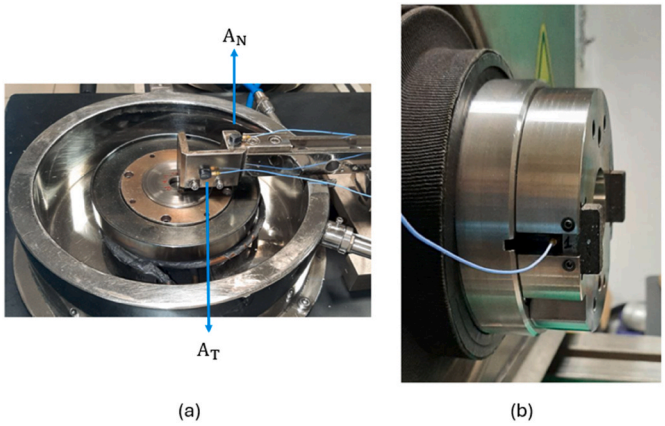

Fig. 6. Vibration measurement setup: (a) Shear accelerometers (A_N and A_T) placed on the pin-holder; (b) triaxial accelerometer placed at the back of a coupon.

The CoF and the particle concentration show a characteristic trace: in the initial stage of the test, they increase up to a peak value, then they decrease, finally entering a steady-state phase. Then, for each test, two characteristic values were identified: a peak and a steady-state value. The difference between steady state and peak emission values is significant for PV factors equal to 3 MPa m/s or greater. For the tests at (1 MPa, 1.5 m/s) no clear peak was observed in the emission curve, even though a minor peak in the CoF was observed. Table 4 lists the peak values of the CoF and particle concentration, along with the sliding distance at which they occur, generally below 600 m. It is interesting to note that the peaks of the total concentration occur at a smaller sliding distance compared to the CoF. The normal and tangential vibrations show different behaviours compared to the friction and particle concentration curves since no clear peaks were observed during the tests (Fig. 8d).

3.2. Subscale dynamometer measurements

Fig. 8 depicts the evolution over time of five parameters for one representative test at (1 MPa, 3 m/s): disc temperature, CoF, particulate emissions, and both components of vibration. A thermal equilibrium was not achieved by the end of the test (Fig. 8a). The final temperatures of the tests are documented in Table 5. The tests conducted at (2 MPa, 3 m/s) approach the maximum temperature of 260 °C, a condition that limited the duration of the tests. The tests at (1 MPa, 3 m/s) exhibit final temperatures surpassing those at (2 MPa, 1.5 m/s), suggesting that the temperature rise in the dynamometer is mainly influenced by V. Also, the CoF does not reach a steady-state (Fig. 8b), since the values are still increasing at the end of the test. This behaviour becomes more evident for the test at (1 MPa, 1.5 m/s).

The time scale of the emission curve in Fig. 8c exceeds the test duration since the acquisition is delayed by 4 s, and it takes about 15 s for the particle concentration to return to its background value (ranging between 4 and 5 #/cm^3). Depending on the sliding velocity, the emission peak occurs at the end of the test or a few seconds earlier, as in the case of Fig. 8, where the peak is reached at 20 s. The sliding distances at which the emission peaks occur are reported in Table 6. Velocity has a role in decreasing the sliding distance at which the peak occurs.

Table 5 summarizes the representative values for all the parameters, in terms of average values and standard deviation among trials. The CoF and the vibrations (RMS) are represented by the final values of the tests. The peak value was considered instead for the particle concentration. The specific wear coefficient is relative to one coupon.

4. Discussion

The observed differences in the behaviors between the two systems will be interpreted based on their distinct characteristics. The thermal aspect is crucial in this study because it impacts the length of the dynamometer tests. Specifically, the duration of these tests was established to match the time it takes for the test at (2 MPa, 3 m/s) to reach a disc temperature of 260 °C. The intention behind this was to maintain mild sliding conditions and prevent the contact temperature from exceeding the TT for emissions. The surface of friction materials is significantly affected by sliding under high contact temperatures, which in turn impacts the performance of brake materials. In particular, the presence of phenolic resin as a binder in the materials causes them to soften as the temperature increases [29]. In addition, the stability of the secondary contact plateaus of the friction layer is highly affected by the contact temperature [30–34], and the wear regime may transition from mild to severe when the temperature exceeds critical values between 300 and 400 °C [35,36]. Finally, regarding the emission, it has been

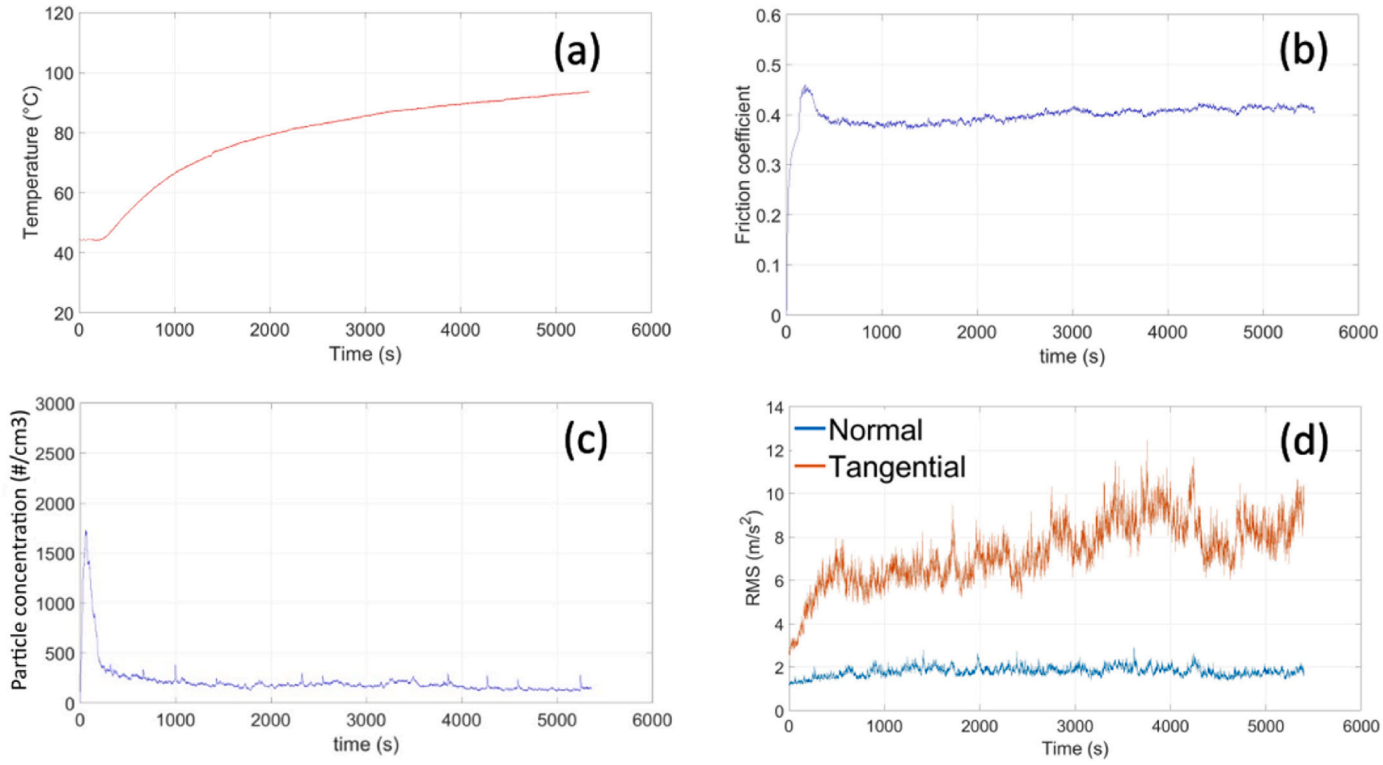

Fig. 7. An example of (a) Temperature, (b) CoF, (c) Emissions, and (d) Vibration trends demonstrated by a PoD test at 1 MPa, 3 m/s.

Table 3
Final disc temperature and steady-state values of the PoD tests.

Testing parameters	Final disc temperature	K_a	CoF	Particle concentration	Normal vibration - RMS	Tangential vibration - RMS
	(°C)	m^2/N	–	#/ cm^3	m/ s^2	m/ s^2
1 MPa, 1.5 m/s	59	(4.3 ± 0.26) e−14	0.51 ± 0.04	670 ± 380	1.3 ± 0.34	2.95 ± 0.2
2 MPa, 1.5 m/s	94.3	(3.2 ± 0.13) e−14	0.47	712 ± 323	2.1 ± 1.3	13.5 ± 9.5
1 MPa, 3 m/s	90.5	(1.75 ± 0.15) e−14	0.42 ± 0.007	230 ± 110	1.6 ± 0.2	5.8 ± 3.8
2 MPa, 3 m/s	142	(1.15 ± 0.2) e−14	0.41 ± 0.04	184 ± 23	15.5 ± 1.7	91 ± 56

Table 4
Peak values of the PoD tests, with the sliding distance at which they occur.

Testing parameters	CoF		Particle concentration	
	–	Sliding distance for the peak (m)	#/ cm^3	Sliding distance for the peak (m)
1 MPa, 1.5 m/s	0.54 ± 0.01	563	715 ± 516	/
2 MPa, 1.5 m/s	0.52 ± 0.01	530 ± 200	1875 ± 35	517 ± 273
1 MPa, 3 m/s	0.47 ± 0.01	361 ± 50	1794 ± 93	165 ± 35
2 MPa, 3 m/s	0.45 ± 0.02	455 ± 15	2731 ± 762	180 ± 40

demonstrated the existence of a TT in the range of 170–190 °C for the PoD and 300–400 °C for the full-scale dynamometers [16,37–39].

The simplified analytical model by Federici et al. [40] is employed to explain the observed differences in temperature evolution between the two testing rigs. This model is referred to as 'modified' because it improves the original modelling approach proposed by Kennedy et al. [41]. This model estimates the average *bulk* temperature rise in the contact region during dry sliding tests in a PoD tribometer. The assumption is that all frictional power is transformed into heat at the contact interface and that there is perfect contact at the disc and disc-holder interface [40]. In this model, the evolution of the surface temperature over time is described by the following equation:

$$T_s(t) = \frac{\mu(t)\, F_N\, v}{\frac{k1}{l1} A_{pin} + h\, A_{disc}^{tot} + m_{disc} \frac{Cp_{disc}}{t}} + T_0 \quad (1)$$

where k_1 is the thermal conductivity of the pin, l_1 is the length of the thermal path of the pin, A_{pin} the nominal contact area of the pin. A_{disc}^{tot} is the total area of the upper surface of the disc, h the heat convection coefficient of the disc, m_{disc} the mass of the disc, and Cp_{disc} the specific heat capacity of cast iron. In addition, T_0 is the starting temperature of the test. Table 7 shows the values of the main parameters of the 'modified' equation for the PoD and the dynamometer. A critical point lied in the evaluation of h, which was evaluated experimentally to get proper values for the systems. The following equation has been exploited:

$$h = \frac{b\, Cp_{disc}\, m_{disc}}{A_s} \quad (2)$$

where A_s is the disc surface area, and b is the coefficient of heat transfer of the Newton's law of cooling, in which the difference in temperature between the body and the environment decays exponentially as a function of time, as follows:

$$T_s(t) = T_r + (T_{max} - T_r)\, e^{-bt} \quad (3)$$

Where T_r is the room temperature, it is assumed that it remains constant

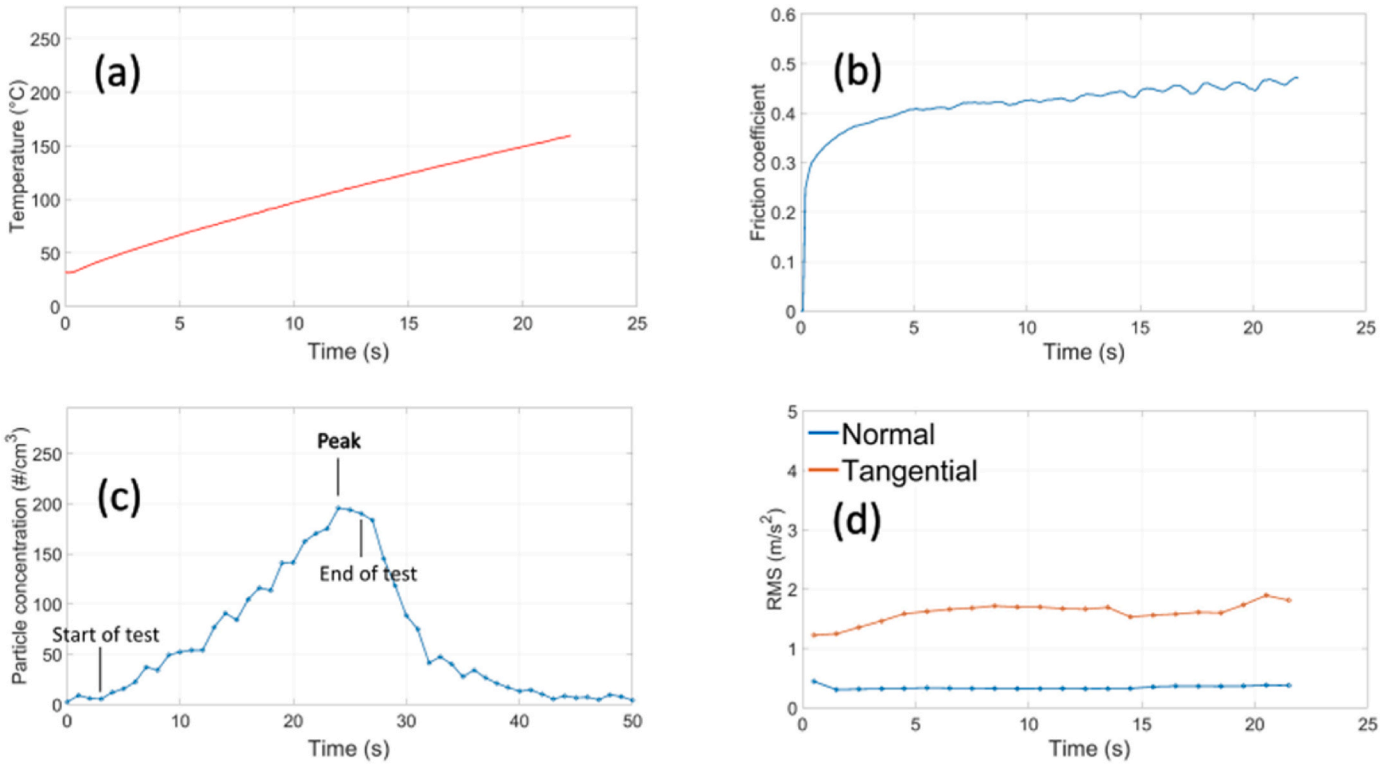

Fig. 8. An example of (a) Temperature, (b) CoF, (c) Emissions, and (d) Vibration trends demonstrated by a dynamometer test at 1 MPa, 3 m/s.

Table 5
Average values of the parameters of the subscale dynamometer.

Testing parameters	Final disc temperature	Ka – coupon	CoF	Particle concentration	Normal vibration - RMS	Tangential vibration - RMS
	°C	m^2/N	–	#/cm^3	m/s^2	m/s^2
1 MPa, 1.5 m/s	82	(1.71 ± 0.01) e−14	0.42 ± 0.02	18.3 ± 3	0.37 ± 0.02	1.9 ± 0
2 MPa, 1.5 m/s	139	(2.53 ± 0.7) e−14	0.43 ± 0.02	92 ± 18	0.35 ± 0.05	2.1 ± 0.3
1 MPa, 3 m/s	153	(1.48 ± 1) e−14	0.45 ± 0.01	225 ± 45	0.4 ± 0.04	1.9 ± 0.3
2 MPa, 3 m/s	259	(3.54 ± 0.6) e−14	0.43 ± 0.01	517 ± 99	0.42 ± 0.013	3 ± 0.04

Table 6
Sliding distance at which the emission peaks occur.

Testing parameters	Total concentration - peak occurrence (m)
1 MPa, 1.5 m/s	14 ± 14
2 MPa, 1.5 m/s	23.5 ± 0.7
1 MPa, 3 m/s	19.5 ± 0.7
2 MPa, 3 m/s	15 ± 1.4

during the heat exchange between the body and the environment, and T_{max} is the initial temperature of the cooling curve. The parameter b was computed from the cooling phase after one test at (1 MPa, 1.5 m/s), maintaining the same angular speed of the disc as during the test, without the friction samples in contact. The cooling curve data were then fitted using an exponential equation.

At the numerator of Eq. (1) is the friction power, $\mu(t)\, F_N\, v$, the product of CoF, nominal contact force and sliding velocity. The friction power is responsible for the contact temperature rise, and, considering the test at (1 MPa, 1.5 m/s), it is higher in the dynamometer by a factor of 7.5. In particular, the normal force applied in the dynamometer tests is 9 times greater than that of the PoD. At the denominator instead, there are three components accountable for the heat dissipation: a conductive component through the pin, a convective component between the disk and the environment, and a heat storage component inside the disc, whose importance decreases linearly over time. After an initial transient

Table 7
Parameters of Eq. (1) and their magnitudes, for the test at 1 MPa, 1.5 m/s.

Parameters	Pin on disc	Dynamometer
k_1 **(W/mK)**	2.4	2.4
l_1 **(m)**	4e-3	5e-3
A_{pin} **(m^2)**	7.85e-5	7.2e-4
A_{disc}^{tot} **(m^2)**	2.7e-2	1.13e-2
m_{disc} **(kg)**	2.8	0.46
Cp_{disc} **(J/Kg·K)**	465	465
F_N **(N)**	79	720
v **(m/s)**	1.51	1.51
μ	0.51	0.42
T_0 **(°C)**	30 °C	30 °C
b **(1/s)**	6.25e-4	4.8e-3
h **(W/ m^2K)**	29.6	88.8
$\mu(t)\, F_N\, v$ **(W)**	61.6	464.4
$\frac{k1}{l1} A_{pin} + h\, A_{disc}^{tot}$ **(W/ K)**	0.85	1.35

the heat storage component becomes negligible, and the constant term given by $\frac{k1}{l1} A_{pin} + h\, A_{disc}^{tot}$ remains the main component for the heat dissipation. Although this component is higher in the dynamometer by a factor of 1.6, it fails to efficiently dissipate the heat generated by the friction power. This qualitatively explains the higher temperature increase in the dynamometer tests.

Figs. 9–11 compare the four output parameters, plotted to pressure

and velocity, both of the pin-on-disc and the dynamometer. Each experimental point is represented by a dot, the average value of three trials, and by a bar, the standard deviation among the same trials.

As mentioned before, the PoD's methodology distinguished peak and steady-state values for emissions and CoF. The PoD tests show higher CoF compared to the dynamometer at 1.5 m/s, namely 15 % for the steady states and 24 % for the peaks. This result can be related to the short duration of the dynamometer tests, which does not allow the tests at 1.5 m/s to reach a proper steady state. CoF values are instead comparable at 3 m/s. Furthermore, the dynamometer shows a slight increase in the CoF moving from 1.5 m/s to 3 m/s, while the PoD shows an evident decrease for both peaks and steady-state values. Even when considering values at the same sliding distance (33 m) for the dynamometer, the CoF remains constant when passing from 1.5 m/s to 3 m/s. The PoD result is in accordance with Wei et al. [42] and Wahlström et al. [43], who showed a decrease in the CoF by increasing both P and V. Candeo et al. [4] instead showed a decrease in CoF as speed increased from 1.8 m/s to 19 m/s, and pressure from 0.3 to 2.5 MPa, in the same subscale dynamometer of this study.

Concerning the wear coefficient K_a, the two systems present no clear correlation in terms of PV sensitivity. The order of magnitude is the same, suggesting a mild wear regime in both cases, however, the dynamometer features higher values at (2 MPa, 3 m/s) and lower values at (1 MPa, 1.5 m/s). Moreover, the wear coefficient in the PoD decreases when P and V increase. This result is again in accordance with Wei et al. [42] and Wahlström et al. [43], who found that both pressure and velocity caused the decrease in the specific wear rate of a low-metallic material sliding against a cast iron disc if the temperature remains below 200 °C. The reason is that P induces better compactness of the secondary plateaus and avoids their detachments from the friction layer, while V decreases the shear force at the plateau region by decreasing the CoF [42]. However, it has to be mentioned that the specific wear coefficient is not properly suitable for the dynamometer tests, as steady states are not reached during the tests, which also explains the high standard deviation in the wear coefficients.

With regard to particulate emissions, a distinction can again be made between steady state and peak values for the PoD. Focusing on peak values, the particle concentration shows a similar trend between the two

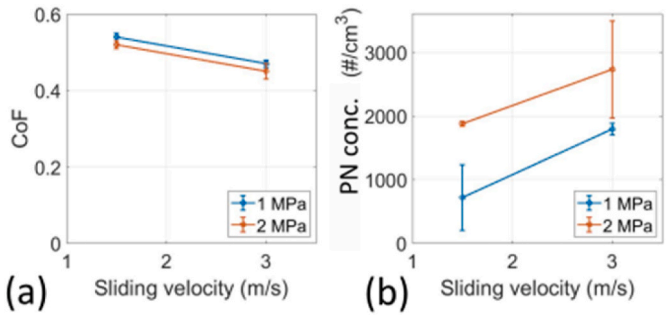

Fig. 10. Peak values of the PoD tests: (a) CoF; (b) Particle number concentration.

systems: it increases with P and V. The steady states of the PoD instead decrease when increasing V. Then it is reasonable to assume that the results of the dynamometer tests are closer to peak values than steady-state values, even if the dynamometer shows a lower sensitivity to pressure at 1.5 m/s. In this regard, Wahlström et al. [25] found that the peaks of coarse particles for a low-metallic material increased with P for a contact temperature below 200 °C. By analysing a pair of materials similar to this study, they showed that the peaks of the concentration increased and became sharper as P increased [25,43,44]. In addition, the absolute values of particle concentration are higher for the PoD peaks by a factor that varies from 5 for the test at (2 MPa, 3 m/s) to 39 for the test at (1 MPa, 1.5 m/s). The particle concentrations calculated at the same sliding distance for the two systems, result to be higher in the PoD by a factor that varies from 2 for the tests at 3 m/s to 5 (or higher) for the tests at 1.5 m/s. This result can be attributed to a scale factor between the two testing rigs and a difference in the measurement setup: even if the same OPS was used, the dynamometer had a higher air flowrate, which dilutes more the concentration, and this effect is not compensated by the smaller area of the pins compared to the coupons. Pearson's correlation coefficient was computed to gain a better understanding of the relationship between the emissions of the two systems. When computed for the PoD peak values and the dynamometer values, this coefficient displayed a high and positive value of 0.89, whereas it remained high but

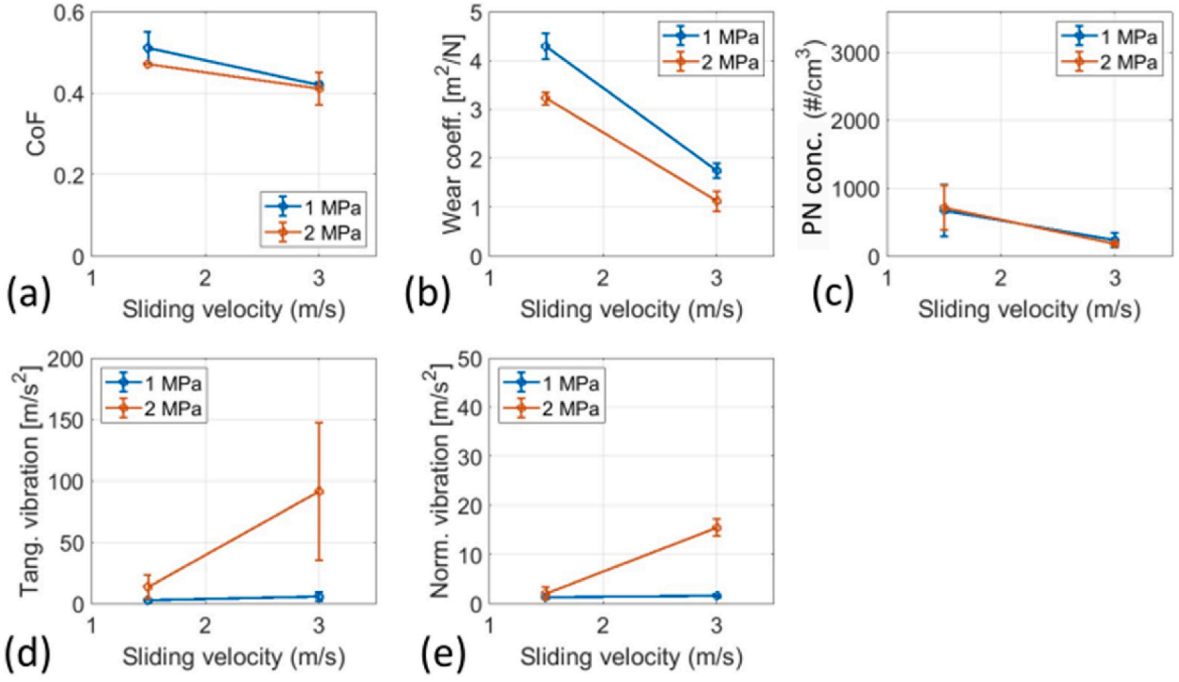

Fig. 9. Steady states of the PoD tests: (a) CoF; (b) Wear coefficient; (c) Particle number concentration; (d) Tangential vibration; and (e) Normal vibration.

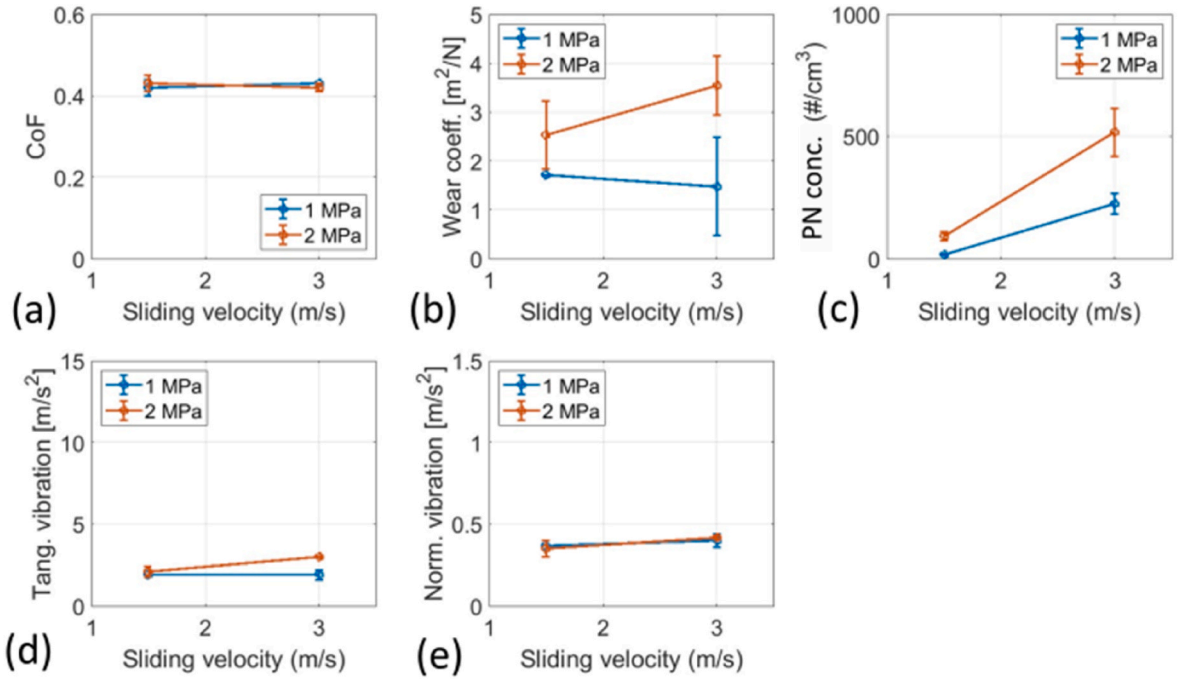

Fig. 11. Dynamometer final values: (a) CoF; (b) Wear coefficient; (c) Particle number concentration; (d) Tangential vibration; and (e) Normal vibration.

became negative, with a value of −0.85, when computed with the PoD steady state values. This result supports the observed stronger correspondence of peak values with dynamometer measurements for particle concentration.

Regarding the vibrations of the two systems, the PoD features higher RMS values than the dynamometer, essentially due to the lower stiffness of its holding system. In both testing rigs, the tangential vibration is higher than the normal component. The ratio between the average tangential and normal vibrations is of the same order of magnitude in the two systems. The dynamometer shows a lower PV sensitivity compared to the PoD, which exhibits higher variation due to its lower stiffness. The approach of linking PM emissions to system vibrations is rather interesting. In a previous study, Jayashree et al. [12] found a relationship between particle number concentration and system vibrations in PoD tests for a simplified friction material. In the current analysis, the steady state of the particle concentration was found to decrease with V and to remain unaffected by P. On the contrary, the tangential and normal vibrations were found to increase with both P and V; however, if we focus on the peak values, a general correlation between the emissions and vibrations is observed. When considering the relationship between vibrations and emissions, particular care should be taken, as both vibration and particle concentration depend on the pressure and velocity conditions. With these considerations in mind, Pearson's correlation coefficients can still be used for comparison purposes. They were computed between the particle number concentration and normal vibrations in the two systems to gain a better understanding of their relationship. For the PoD, a coefficient around 0.5 indicates an intermediate correlation in terms of PV sensitivity between the two parameters. Conversely, the correlation coefficient for the dynamometer is approximately 0.9, denoting a higher correlation.

An area of particular interest for future research remains the relationship between vibration and particulate emissions. Specific tests on various types of friction materials should be conducted to better investigate this relationship in both testing scales. Additionally, modal analysis should be considered to quantify the stiffness of the two systems and correlate it with the different values of root mean square (RMS) acceleration.

5. Conclusions

This study compared the CoF, wear, PM emissions, and system vibrations between a PoD and a reduced-scale dynamometer, aiming to enhance the interpretation of the testing results and their relevance to the related fields of application. The main outcomes regarding the applied methodology and investigated behaviours are as follows:

1. Dragging conditions were selected to facilitate comparison between the two testing rigs. The higher increase in disc temperature of the reduced-scale dynamometer was primarily caused by higher energy input. Testing conditions included 1 and 2 MPa contact pressure, sliding velocities of 1.5 and 3 m/s, and a disc temperature below 260 °C.
2. Although the two systems exhibited similar values of CoF, the PoD displayed PV sensitivity, whereas the CoF on the dynamometer remained relatively constant. This difference can be attributed to the distinct thermal behaviours of each system and the absence of steady states in the dynamometer system.
3. K_a values were typical of mild wear regimes, 1–4 e−14 m^2/N in both systems; however, steady states were not achieved in the reduced-scale dynamometer.
4. The particulate concentration of the dynamometer tests better correlated to the peak phases of the PoD tests.
5. PoD exhibited higher RMS vibrations due to its lower stiffness, while both systems displayed higher tangential vibration components.
6. When performing pin-on-disc testing, it becomes important to consider not only the steady state values, but also the peak, or transition, phases.

CRediT authorship contribution statement

Domenico Antonio Rita: Writing – original draft, Methodology, Formal analysis, Data curation. **Stefano Candeo:** Writing – review & editing, Supervision. **Priyadarshini Jayashree:** Writing – review & editing. **Ana Paula Gomes Nogueira:** Writing – review & editing, Supervision. **Emiliano Rustighi:** Writing – review & editing, Validation, Supervision, Methodology. **Giovanni Straffelini:** Writing – review &

editing, Validation, Supervision, Methodology.

Declaration of competing interest

The authors declare that they have no known competing financial interests or personal relationships that could have appeared to influence the work reported in this paper.

Data availability

Data will be made available on request.

References

[1] G. Straffelini, Friction and Wear: Methodologies for Design and Control, Springer International Publishing, Cham, 2015, https://doi.org/10.1007/978-3-319-05894-8.

[2] P.G. Sanders, T.M. Dalka, R.H. Basch, A reduced-scale brake dynamometer for friction characterization, Tribol. Int. 34 (2001) 609–615, https://doi.org/10.1016/S0301-679X(01)00053-6.

[3] J. Park, B. Joo, H. Seo, W. Song, J.J. Lee, W.K. Lee, H. Jang, Analysis of wear induced particle emissions from brake pads during the worldwide harmonized light vehicles test procedure (WLTP), Wear 466–467 (2021) 203539, https://doi.org/10.1016/j.wear.2020.203539.

[4] S. Candeo, M. Federici, M. Leonardi, G. Straffelini, Brake performance maps for a Cu-free friction material with different scorching conditions, Tribol. Trans. 64 (2021) 540–550, https://doi.org/10.1080/10402004.2020.1869360.

[5] F. Varriale, S. Candeo, G. Riva, J. Wahlström, Y. Lyu, A brake system coefficient of friction estimation using 3D friction maps, Lubricants 10 (2022) 134, https://doi.org/10.3390/lubricants10070134.

[6] N. Perzborn, C. Agudelo, G.P. Ostermeyer, On similarities and differences of measurements on inertia dynamometer and scale testing tribometer for friction coefficient evaluation, SAE International Journal of Materials and Manufacturing 8 (2015) 104–117.

[7] M.S. Balaji, K. Jitendra, E. Arumugam, B.P. Sethupathi, State of the art on challenges for friction material manufacturers – raw materials, regulations, environmental, and NVH aspects, Proc. IME J. J. Eng. Tribol. 237 (2023) 926–942, https://doi.org/10.1177/13506501221135071.

[8] F. Amato (Ed.), Non-exhaust Emissions: an Urban Air Quality Problem for Public Health: Impact and Mitigation Measurs, Academic Press, London San Diego, CA Cambridge, MA Oxford, 2018.

[9] K. Katsouyanni, G. Touloumi, E. Samoli, A. Gryparis, A. Le Tertre, Y. Monopolis, G. Rossi, D. Zmirou, F. Ballester, A. Boumghar, H.R. Anderson, B. Wojtyniak, A. Paldy, R. Braunstein, J. Pekkanen, C. Schindler, J. Schwartz, Confounding and effect modification in the short-term effects of ambient particles on total mortality: results from 29 European cities within the APHEA2 project, Epidemiology 12 (2001) 521–531, https://doi.org/10.1097/00001648-200109000-00011.

[10] J.M. Samet, F. Dominici, F.C. Curriero, I. Coursac, S.L. Zeger, Fine particulate air pollution and mortality in 20 U.S. cities, 1987-1994, N. Engl. J. Med. 343 (2000) 1742–1749, https://doi.org/10.1056/NEJM200012143432401.

[11] C.A. Pope, R.T. Burnett, M.J. Thun, E.E. Calle, D. Krewski, K. Ito, G.D. Thurston, Lung cancer, cardiopulmonary mortality, and long-term exposure to fine particulate air pollution, JAMA 287 (2002) 1132–1141, https://doi.org/10.1001/jama.287.9.1132.

[12] P. Jayashree, E. Rustighi, G. Straffelini, A novel study on the reduction of non-exhaust particulate matter emissions through system vibration control, Sci. Rep. 12 (2022) 7478, https://doi.org/10.1038/s41598-022-11703-w.

[13] P. Jayashree, G. Fredi, E. Rustighi, A.P. Gomes Nogueira, G. Straffelini, Effect of internal and external damping in the reduction of non-exhaust particulate matter emissions in a low metallic friction material formulation, Wear 544–545 (2024) 205292, https://doi.org/10.1016/j.wear.2024.205292.

[14] L. Wei, Y.S. Choy, C.S. Cheung, H.K. Chu, Comparison of tribology performance, particle emissions and brake squeal noise between Cu-containing and Cu-free brake materials, Wear 466–467 (2021) 203577, https://doi.org/10.1016/j.wear.2020.203577.

[15] D. Veeman, J.K. Katiyar, A. Ruggiero, Tribo-mechanical performance of brake composite material: a comprehensive review, Tribology - materials, Surface. Interfac. 17 (2023) 271–294, https://doi.org/10.1080/17515831.2023.2211819.

[16] M. Alemani, J. Wahlström, V. Matějka, I. Metinöz, A. Söderberg, G. Perricone, U. Olofsson, Scaling effects of measuring disc brake airborne particulate matter emissions – a comparison of a pin-on-disc tribometer and an inertia dynamometer bench under dragging conditions, Proc. IME J. J. Eng. Tribol. 232 (2018) 1538–1547, https://doi.org/10.1177/1350650118756687.

[17] M. Federici, M. Alemani, C. Menapace, S. Gialanella, G. Perricone, G. Straffelini, A critical comparison of dynamometer data with pin-on-disc data for the same two friction material pairs – a case study, Wear 424–425 (2019) 40–47, https://doi.org/10.1016/j.wear.2019.02.009.

[18] P. Jayashree, G. Straffelini, The influence of the addition of aluminum anodizing waste on the friction and emission behavior of different kinds of friction material formulations, Tribol. Int. 173 (2022) 107676, https://doi.org/10.1016/j.triboint.2022.107676.

[19] V. Matějka, M. Leonardi, P. Praus, G. Straffelini, S. Gialanella, The role of graphitic carbon nitride in the formulation of copper-free friction composites designed for automotive brake pads, Metals 12 (2022) 123, https://doi.org/10.3390/met12010123.

[20] "Dynamometer Global Brake Effectiveness," SAE Paper No. J2522, 2014 n.d.).

[21] J.F. Archard, Friction between metal surfaces, Wear 113 (1986) 3–16, https://doi.org/10.1016/0043-1648(86)90052-9.

[22] J.F. Archard, Contact and rubbing of flat surfaces, J. Appl. Phys. 24 (1953) 981–988, https://doi.org/10.1063/1.1721448.

[23] A.P. Gomes Nogueira, D. Carlevaris, C. Menapace, G. Straffelini, Tribological and emission behavior of novel friction materials, Atmosphere 11 (2020) 1050, https://doi.org/10.3390/atmos11101050.

[24] P. Jayashree, A. Sinha, S. Gialanella, G. Straffelini, Dry sliding behavior and particulate emissions of a SiC-graphite composite friction material paired with HVOF-coated counterface, Atmosphere 13 (2022) 296, https://doi.org/10.3390/atmos13020296.

[25] J. Wahlström, L. Olander, U. Olofsson, A pin-on-disc study focusing on how different load levels affect the concentration and size distribution of airborne wear particles from the disc brake materials, Tribol. Lett. 46 (2012) 195–204, https://doi.org/10.1007/s11249-012-9944-5.

[26] U. Olofsson, L. Olander, A. Jansson, A study of airborne wear particles generated from a sliding contact, J. Tribol. 131 (2009), https://doi.org/10.1115/1.3176990.

[27] J. Wahlström, Y. Lyu, V. Matjeka, A. Söderberg, A pin-on-disc tribometer study of disc brake contact pairs with respect to wear and airborne particle emissions, Wear 384–385 (2017) 124–130, https://doi.org/10.1016/j.wear.2017.05.011.

[28] S. Candeo, A.P. Nogueira, M. Leonardi, G. Straffelini, A study of friction, wear and particulate emissions during the bedding stage of a Cu-free friction material, Wear 486–487 (2021) 204095, https://doi.org/10.1016/j.wear.2021.204095.

[29] J.G. Balotin, P.D. Neis, N.F. Ferreira, Analysis of the Influence of Temperature on the Friction Coefficient of Friction Materials, vol. 4, 2009.

[30] W. Österle, I. Urban, Third body formation on brake pads and rotors, Tribol. Int. 39 (2006) 401–408, https://doi.org/10.1016/j.triboint.2005.04.021.

[31] C. Piyush, P. Verma, L. Menapace, A. Bonfanti, R. Ciudin, S. Gialanella, G. Straffelini, Braking pad-disc system: wear mechanisms and formation of wear fragments, Wear 322–323 (2015) 251–258, https://doi.org/10.1016/j.wear.2014.11.019.

[32] G. Straffelini, P. Verma, I. Metinoz, R. Ciudin, G. Perricone, S. Gialanella, Wear behavior of a low metallic friction material dry sliding against a cast iron disc: role of the heat-treatment of the disc, Wear 348–349 (2015) 10–16, https://doi.org/10.1016/j.wear.2015.11.020.

[33] M. Eriksson, S. Jacobson, Tribological surfaces of organic brake pads, Tribol. Int. 33 (2000) 817–827, https://doi.org/10.1016/S0301-679X(00)00127-4.

[34] M.G. Jacko, P.H.S. Tsang, S.K. Rhee, Wear debris compaction and friction film formation of polymer composites, Wear 133 (1989) 23–38, https://doi.org/10.1016/0043-1648(89)90110-5.

[35] P.V. Gurunath, J. Bijwe, Friction and wear studies on brake-pad materials based on newly developed resin, Wear 263 (2007) 1212–1219, https://doi.org/10.1016/j.wear.2006.12.050.

[36] A.E. Anderson, Friction and Wear of Automotive Brakes, ASM International, 1992.

[37] M. Alemani, U. Olofsson, G. Perricone, A. Söderberg, J. Wahlström, A. Ciotti, A Study on the Load Level Influence on Particulate Matter Emissions from the Sliding Contact between a Low Steel Friction Material and Cast Iron, 2015.

[38] M. Alemani, J. Wahlström, U. Olofsson, On the influence of car brake system parameters on particulate matter emissions, Wear 396–397 (2018) 67–74, https://doi.org/10.1016/j.wear.2017.11.011.

[39] J. Kukutschová, P. Moravec, V. Tomášek, V. Matějka, J. Smolík, J. Schwarz, J. Seidlerová, K. Safářová, P. Filip, On airborne nano/micro-sized wear particles released from low-metallic automotive brakes, Environ. Pollut. 159 (2011) 998–1006, https://doi.org/10.1016/j.envpol.2010.11.036.

[40] M. Federici, G. Straffelini, S. Gialanella, Pin-on-Disc testing of low-metallic friction material sliding against HVOF coated cast iron: modelling of the contact temperature evolution, Tribol. Lett. 65 (2017) 121, https://doi.org/10.1007/s11249-017-0904-y.

[41] F.E. Kennedy, Y. Lu, I. Baker, Contact temperatures and their influence on wear during pin-on-disk tribotesting, Tribol. Int. 82 (2015) 534–542, https://doi.org/10.1016/j.triboint.2013.10.022.

[42] L. Wei, Y.S. Choy, C.S. Cheung, A study of brake contact pairs under different friction conditions with respect to characteristics of brake pad surfaces, Tribol. Int. 138 (2019) 99–110, https://doi.org/10.1016/j.triboint.2019.05.016.

[43] J. Wahlström, V. Matejka, Y. Lyu, A. Söderberg, Contact pressure and sliding velocity maps of the friction, wear and emission from a low-metallic/cast-iron disc brake contact pair, Tribol. Ind. 39 (2017) 460–470, https://doi.org/10.24874/ti.2017.39.04.05.

[44] J. Wahlström, A. Söderberg, L. Olander, U. Olofsson, A disc brake test stand for measurement of airborne wear particles, Lubric. Sci. 21 (2009) 241–252.